Continuously tunable topological pump in high-dimensional cold atomic gases

Yan-Bin Yang,[1] L.-M. Duan,[1,2] and Yong Xu[1,*]

[1]*Center for Quantum Information, IIIS, Tsinghua University, Beijing 100084, People's Republic of China*

[2]*Department of Physics, University of Michigan, Ann Arbor, Michigan 48109, USA*

(Received 4 February 2018; revised manuscript received 4 August 2018; published 17 October 2018)

Controllability of ultracold atomic gases has reached an unprecedented level, allowing for experimental realization of the long-sought-after Thouless pump, which can be interpreted as a dynamical quantum Hall effect. On the other hand, Weyl semimetals and Weyl nodal-line semimetals with touching points and rings in band structures have sparked tremendous interest in various fields in the past few years. Here, we show that dynamical Weyl points and dynamical four-dimensional (4D) Weyl nodal rings, which are protected by the first Chern number on a parameter surface formed by quasimomentum and time, emerge in a two-dimensional and three-dimensional system, respectively. We find that these dynamical topological gapless phenomena lead to a topological pump and the amount of pumped particles is not quantized and can be continuously tuned by controlling experimental parameters over a wide range, in stark contrast with the Thouless pump with quantized transport, which does not allow for such continuous tuning. We also propose an experimental scheme to realize the dynamical Weyl points and dynamical 4D Weyl nodal rings and to observe their corresponding topological pump in cold atomic gases.

DOI: 10.1103/PhysRevB.98.165128

I. INTRODUCTION

Recently, topological gapless phenomena have seen a rapid advance in three-dimensional (3D) condensed-matter systems ranging from solid-state materials [1–8] and cold atoms [9–17] to optical and acoustic systems [18,19]. This is mainly attributed to their powerful ability to simulate fundamental physics [20–22]. For instance, Weyl fermions, which have been long sought after in particle physics, have recently been experimentally observed in condensed-matter systems [23–27]. These fermions correspond to the gapless touching points in the energy band with linear dispersion along all directions. Because they are protected by the first Chern number, they can also be viewed as the quantum Hall phase-transition points in momentum space, leading to an anomalous Hall effect [22]. Another celebrated example of a 3D gapless phenomenon is the Weyl nodal ring [28–31], which has also been experimentally observed recently [29]. Even though they are topologically protected by the quantized Berry phase, the anomalous Hall effect cannot occur in this system in the absence of external magnetic fields.

On the other hand, Thouless predicted the quantized transport of particles arising from a cyclic deformation of an underlying Hamiltonian without an applied bias voltage [32], which has recently been observed in cold atom experiments [33,34], thanks to rapid progress of cold atom technology. Such a quantized transport can be interpreted as the dynamical quantum Hall effect [34,35] on a surface formed by quasimomentum and time. Given that the anomalous Hall effect occurs in Weyl semimetals, a natural question to ask is whether a dynamical Weyl point featuring a topological transport, which can be interpreted as a dynamical anomalous Hall effect, exists in a two-dimensional (2D) material. Since Weyl nodal semimetals in 3D do not support the anomalous Hall effect, we do not expect the existence of a dynamical Weyl nodal ring. However, in a 3D system, viewing time as a parameter, one may wonder whether a new dynamical gapless phenomenon featuring the topological transport appears.

In this paper, we demonstrate that the dynamical Weyl points can be engineered in a 2D slowly periodically driven system. Here, besides two quasimomenta, e.g., k_x and k_y, time t may be regarded as an artificial parameter, taking the place of another quasimomentum parameter k_z. When the adiabatic condition is fulfilled, the Weyl point can be characterized by the Chern number defined on a closed surface in the space (k_x, k_y, t) enclosing the point. Alternatively, because of the periodicity of the system, it ends up with the same state over a cycle, implying that the system at time t is equivalent to that at time $t + T$ with T being the period, reminiscent of the property of a Brillouin zone. Hence, the Chern number can be defined on a torus (k_x, t) like in the momentum space. In a 3D system, adding time as a parameter gives us a four-dimensional (4D) system, and in the 4D space we propose a new gapless ring named dynamical 4D Weyl nodal ring protected by the first Chern number, which is different from a Weyl nodal ring in the 3D space protected by a quantized Berry phase [28,30,31].

Remarkably, we find that the dynamical Weyl points and the dynamical 4D Weyl nodal rings give rise to a nonquantized topological pump [as schematically illustrated in Fig. 1(a)] and the number of pumped particles can be continuously tuned by controlling the experimental parameters, similar to the classical Archimedes screw that can be tuned by tilting the screw, even though the physics underlying our system is quantum mechanics and topology. Finally, we propose an

*yongxuphy@tsinghua.edu.cn

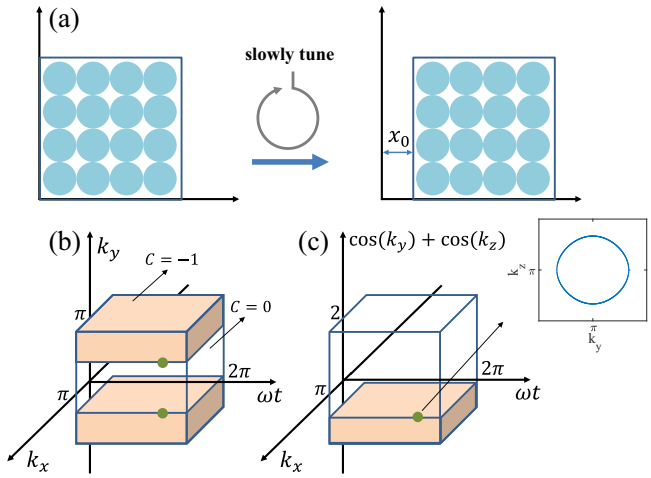

FIG. 1. Schematic of 2D pumping and locations of dynamical Weyl points and dynamical 4D Weyl nodal rings. (a) Sketch of pumping particles in 2D by slowly varying parameters of a system without a bias, where the average displacement of a cloud of atoms over an entire cycle is denoted by x_0. (b), (c) Distribution of the Chern number defined in the $(k_x, \omega t)$ plane as a function of k_y in 2D and $\cos(k_y)+\cos(k_z)$ in 3D, respectively. The Chern number is -1 in the light orange regions and 0 in other regions. The green points in panels (b) and (c) represent the dynamical Weyl points and dynamical 4D Weyl nodal rings [shown in the inset in panel (c)], respectively; they separate the topological trivial and nontrivial phases. In panel (b), $\lambda = 1$ and $M_0 = 2$. In panel (c), $\lambda = 1$ and $M_0 = 3$.

experimental scheme to realize the dynamical Weyl points and dynamical 4D Weyl nodal rings and to observe their corresponding tunable topological pump in cold atomic gases.

II. MODEL HAMILTONIAN

Consider a toy model that is described by the following time-dependent Hamiltonian in momentum space:

$$H(\mathbf{k}, t) = -\sin(k_x)\sigma_x + \lambda\cos(\omega t)\sigma_y + [M + \cos(k_x) + \lambda\sin(\omega t)]\sigma_z, \quad (1)$$

where k_x is the quasimomentum in the x direction, σ_ν with $\nu = x, y, z$ are the Pauli matrices, and λ is a real parameter (we take $\lambda > 0$ for simplicity). Here, $M = M_0 + \cos(k_y)$ with M_0 being a real parameter in 2D and $M = M_0 + \cos(k_y) + \cos(k_z)$ in 3D, where k_y and k_z are the quasimomenta in the y and z directions, respectively. The unit of energy and length is taken to be 1. The Hamiltonian is time dependent and periodic with $H(\mathbf{k}, t + T) = H(\mathbf{k}, t)$ and $T = 2\pi/\omega$.

Provided $M = M_0$, this Hamiltonian is a typical model of a Chern band [36] in the (k_x, k_y) space if ωt is replaced with k_y. Instead, we define the Chern number in (k_x, t) space for the nth instantaneous band as

$$C_n(M) = \frac{1}{2\pi}\int_{-\pi}^{\pi} dk_x \int_0^T dt\,\Omega_n(k_x, t), \quad (2)$$

where t takes the place of a quasimomentum, and the Berry curvature [37] is $\Omega_n(k_x, t) = -2\mathrm{Im}(\langle\partial_{k_x}\mathrm{u_n(k_x, t)}|\partial_t\mathrm{u_n(k_x, t)}\rangle)$ with $|u_n(k_x, t)\rangle$ being the nth instantaneous eigenstate of $H(\mathbf{k}, t)$, i.e., $H(\mathbf{k}, t)|u_n(k_x, t)\rangle = E_n(k_x, t)|u_n(k_x, t)\rangle$.

By straightforward calculation, we find $C_1 = 1$ if $-(1+\lambda) < M < -|1-\lambda|$, $C_1 = -1$ if $|1-\lambda| < M < 1+\lambda$, and zero otherwise. In 2D, the Chern number changes abruptly with respect to k_y, implying a transition between different dynamical quantum Hall phases in the momentum space. The transition point may therefore be called the dynamical Weyl point. These points are located at $[k_x^W = 0, k_y^W = \alpha\arccos(-1 - M_0 \mp \lambda), \omega t = \pm\pi/2]$ with $\alpha = \pm 1$ when $-2 \mp \lambda < M_0 < \mp\lambda$, and at $[k_x^W = \pi, k_y^W = \alpha\arccos(1 - M_0 \mp \lambda), \omega t = \pm\pi/2]$ when $\mp\lambda < M_0 < 2 \mp \lambda$. For instance, when $\lambda = 1$ and $M_0 = 2$, with the second condition being satisfied, there appear two gapless points located at $(k_x^W = \pi, k_y^W = \pm\pi/2, \omega t = 3\pi/2)$, as shown in Fig. 1(b). These points correspond to the abrupt change of the Chern number along k_y, i.e., $C_1 = -1$ when $|k_y| > \pi/2$ and $C_1 = 0$, otherwise, as displayed in Fig. 1(b). Alternatively, one may choose a closed surface enclosing the point and find its Chern number equal to ± 1.

In 3D, viewing t as a parameter, we have a 4D space characterized by $(\mathbf{k}, t)$. We find gapless rings lying in the $(k_x^W = 0, \omega t = \pm\pi/2)$ plane when $-3 \mp \lambda < M_0 < 1 \mp \lambda$ or in the $(k_x^W = \pi, \omega t = \pm\pi/2)$ plane when $-1 \mp \lambda < M_0 < 3 \mp \lambda$. For example, when $\lambda = 1$ and $M_0 = 3$, a single gapless ring appears in the (k_y, k_z) plane corresponding to $k_x = \pi$, $\omega t = 3\pi/2$, and $\cos(k_y) + \cos(k_z) = -1$, as illustrated in Fig. 1(c). Compared to a Weyl nodal ring that is protected by the quantized Berry phase [28,30,31], this ring is characterized by the first Chern number over a 2D closed surface that encloses a single gapless point on the ring. For instance, by fixing $k_z = \pi$ for the ring shown in Fig. 1(c), we reduce the Hamiltonian from the 4D space to a 3D one that is identical to the case shown in Fig. 1(b) and hence choosing a 2D closed surface to wrap up a single gapless point yields a quantized Chern number. We dub the gapless ring a dynamical 4D Weyl nodal ring. In Fig. 1(c), we also show that the ring corresponds to the topological phase transition of dynamical quantum Hall effects. Inside a ring for a fixed (k_y, k_z), the Chern number over the $(k_x, \omega t)$ torus is -1; outside the ring, it is 0.

III. TOPOLOGICAL PUMP

With the dynamical Weyl points and dynamical 4D Weyl nodal rings, we are now ready to study the topological pump in these systems. The number of pumped particles per unit length in 2D or per unit area in 3D is given by [37]

$$N_p = \sum_n \int_0^T dt \int_{BZ} \frac{d\mathbf{k}}{(2\pi)^d}\langle\psi_n(\mathbf{k}, t)|\hat{v}_x|\psi_n(\mathbf{k}, t)\rangle, \quad (3)$$

where $\hat{v}_x = \partial_{k_x}H(\mathbf{k}, t)$ is the velocity operator, d is the dimension of a system, and $|\psi_n(\mathbf{k}, t)\rangle$ is the evolution of a state initialized to the nth eigenstate of $H(\mathbf{k}, 0)$; the integral in the momentum space is over a Brillouin zone and $\sum_n$ is the summation over the filled bands.

With the assumption of the adiabatic condition (i.e., ω is sufficiently small), by time-dependent perturbation theory, the

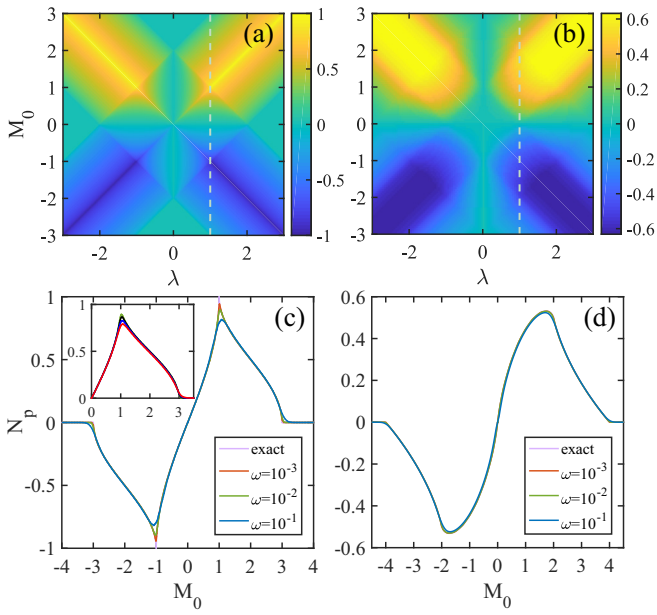

FIG. 2. Amount of pumped particles. Amount of pumped particles (a) per unit length in 2D and (b) per unit area in 3D with respect to λ and M_0. The results are obtained under the adiabatic condition. Amount of pumped particles (c) per unit length in 2D and (d) per unit area in 3D for $\lambda = 1$, which are numerically calculated for $\omega = 0.001$, 0.01, 0.1. The exact result corresponds to the case with $\omega \to 0$. The inset in panel (c) plots the results for $\omega = 0.01$ and the dephasing rate $\gamma = 0$, 0.05, 0.1, 0.15 as the green, black, blue, and red lines, respectively.

formula above can be reduced to

$$N_p = -\sum_n \int_{BZ'} \frac{d\mathbf{k}'}{(2\pi)^{d-1}} C_n(\mathbf{k}'), \tag{4}$$

where the integration is performed over the momentum space except k_x. In one dimension (1D), it corresponds to the celebrated result obtained by Thouless [32]. In higher dimensions, the formula indicates that the amount of pumped particles is dictated by the length in 2D (area in 3D) with corresponding Chern numbers. As a consequence, the amount is not necessarily quantized and its value can be tuned by changing the length in 2D and area in 3D. In our toy model, it is determined by M_0 and λ. For example, in 2D, the amount depends on the distance between two dynamical Weyl points along k_y.

To demonstrate how the pump can be tuned, we plot the amount of pumped particles per unit length in 2D and per unit area in 3D over a cycle with respect to M_0 and λ in Fig. 2. In the ideal case with an infinitesimal ω, the amount can be tuned from -1 to 1 in 2D and from -0.63 to 0.63 in 3D. It is symmetric and antisymmetric with respect to $\lambda = 0$ and $M_0 = 0$, respectively; the antisymmetry reflects the flip of the charge of the dynamical Weyl points and dynamical 4D Weyl nodal rings. Because of the presence of these gapless points (or rings), one may wonder whether the excitation near the gapless regions would compromise our results. To check this, we perform the numerical calculation of the amount of pumped particles by using distinct finite ω for $\lambda = 1$, based on Eq. (3), where $|\psi_n(\mathbf{k}, t)\rangle$ is calculated by solving the Schrödinger equation supposing that the states are initialized to the ground states of $H(\mathbf{k}, 0)$. The results are plotted in Figs. 2(c) and 2(d), showing that the influence on the transport over a cycle is very small in most parts except in the vicinity of $M_0 = \pm 1$, ± 3, where $N_p = \pm 1$, 0 in 2D, and in almost the whole region in 3D, even when $\omega = 0.1$. The nonadiabaticity effects are directly related to the probability that particles are excited to the higher band near the gap-closing region. Around these regions, the Hamiltonian is approximated by $H = -\sin(k_x)\sigma_x + [M \pm 1 + \cos(k_x)]\sigma_z \mp \omega\delta t\sigma_y$, where δt is measured with respect to $t = \pm\pi/(2\omega)$. According to the Landau–Zener formula, the total number of excited particles into a higher band is given by $N_e \approx \int_0^\infty dE D(E) P(E)$, where $D(E)$ is the density of states and $P(E) = e^{-\pi E^2/\omega}$. In 2D, when $M_0 = 1$ or $M_0 = 3$, with $E \approx [\delta k_x^2 + (\delta k_x^2 \pm \delta k_y^2)^2/4]^{1/2}$ near the gapless points, we can qualitatively assume $E \approx (\delta k_x^2 + \delta k_y^4/4)^{1/2}$ (which is fulfilled when $\delta k_y \gg \delta k_x$) and find $D(E) \propto \sqrt{E}$. Yet, in other regions, $E \approx [\delta k_x^2 + \sin(k_y^W)^2 \delta k_y^2]^{1/2}$ and $D(E) \propto E$. Apparently, the number of excited particles in the former case is larger than that in the latter near zero energy because of higher density of states, leading to the manifest nonadiabaticity effects. For a dynamical 4D Weyl nodal ring in a 3D system, the nonadiabaticity effects are also small since $D(E) \propto E$.

IV. DEPHASING EFFECT

In a realistic cold atom experiment, a dephasing may appear naturally due to laser noise. To see whether the topological pump is stable against dephasing, which randomizes the coherent superposition of excited and ground states, we solve a minimal pure-dephasing model described by the following master equation in the Lindblad form [38]:

$$\dot{\rho}_\mathbf{k} = -i[H(\mathbf{k}, t), \rho_\mathbf{k}] + \gamma(\bar{\sigma}_z(t)\rho_\mathbf{k}\bar{\sigma}_z(t) - \rho_\mathbf{k}), \tag{5}$$

where $\rho_\mathbf{k}$ is the density matrix, γ is the dephasing rate, $\bar{\sigma}_z(t) = \mathbf{d}(t)\cdot\boldsymbol{\sigma}/d(t)$ if the Hamiltonian is written as $H = \mathbf{d}(t)\cdot\boldsymbol{\sigma}$. Here, we have adopted a simplest pure-dephasing model where the Lindblad operator $\bar{\sigma}_z(t)$ is assumed to always commute with the Hamiltonian $H(\mathbf{k}, t)$. In the inset of Fig. 2(c), we plot the amount of pumped particles per unit length over a cycle in the 2D case as a function of M_0 for $\lambda = 1$. The transport is only slightly reduced for small dephasing rates in most parts and this reduction increases with γ as dephasing decreases the transported amount in each 1D insulator with a fixed k_y [39]. The reduction is especially manifest around $M_0 = 1$, where more particles near the gapless point are excited to the higher band; these particles lose their coherence by dephasing and lead to strong suppression of the transport.

V. EXPERIMENTAL REALIZATION

To realize the dynamical Weyl points and dynamical 4D Weyl nodal rings and their corresponding tunable topological pump, we consider the following continuous model:

$$H_C = \frac{\mathbf{p}^2}{2m} - \sum_v V_v \cos^2(k_{Lv} r_v) + h_z\sigma_z + V_N\sigma_y, \tag{6}$$

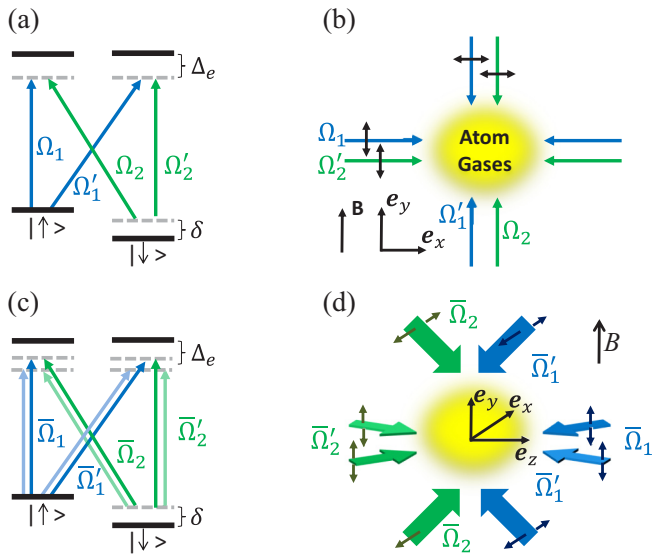

FIG. 3. Laser configurations. Sketch of laser configurations to realize (a), (b) dynamical Weyl points and (c), (d) dynamical 4D Weyl nodal rings. The laser beams denoted by the same color arrows possess the same frequency. The laser beam denoted by the green arrow is generated by applying an acoustic-optical modulator (AOM) to the other laser beam. The double arrows describe the linear polarization direction of laser beams. **B** is the magnetic field and δ is the double photon detuning. In panel (c), the laser beams with the light colors correspond to those with Rabi frequencies $\tilde{\Omega}_n$ and $\tilde{\Omega}'_n$ with $n = 1, 2$. In panel (d), the configuration of these lasers is the same as those plotted and thus neglected for clarity.

where m is the mass of atoms, $\mathbf{p} = -i\hbar\nabla$ is the momentum operator, h_z is the Zeeman field, $V_\nu > 0$ with $\nu = x, y$ in 2D ($\nu = x, y, z$ in 3D) denote the strength of optical lattices with the lattice constants being $a_\nu = \pi/k_{L\nu}$, and $V_N = V_{\mathrm{SO}} + V_{Zy}$ with $V_{\mathrm{SO}} = \Omega_{\mathrm{SO}} \sin(k_{Lx}r_x)\cos(k_{Ly}r_y)$ and $V_{Zy} = -V_{Zy0}\cos(k_{Ly}r_y)\cos(k_{Lx}r_x)$ in 2D [$V_{\mathrm{SO}} = \Omega_{\mathrm{SO}}\sin(k_{Lx}r_x)\cos(k_{Ly}r_y)\cos(k_{Lz}r_z)$ and $V_{Zy} = -V_{Zy0}\cos(k_{Ly}r_y)\cos(k_{Lx}r_x)\cos(k_{Lz}r_z)$ in 3D]. This model gives us the tight-binding Hamiltonian in momentum space (see Methods for details)

$$H(\mathbf{k}) = (h_z + h_t)\sigma_z - 2J_{\mathrm{SO}}\sin(k_x a_x)\sigma_x + h_y\sigma_y, \quad (7)$$

where $h_t = 2\sum_\nu J_\nu \cos(k_\nu a_\nu)$ with ν being summed over x and y in 2D (x, y, and z in 3D). By slowly driving the Hamiltonian according to $h_y = \lambda\cos(\omega t)$ and $h_z = M_0 + \lambda\sin(\omega t)$, we achieve the toy model in Eq. (1).

To engineer the continuous model in Eq. (6) in experiments, we can apply the current experimental technology that implements the 2D spin-orbit coupling in cold atomic gases [40–42], where the spin is represented by two hyperfine states of alkali-metal atoms such as ^{40}K [43,44] and ^{87}Rb [40,41]. In Figs. 3(a) and 3(b), we plot a schematic of a simple and feasible laser configuration scheme for realization of the dynamical Weyl points exhibiting the tunable topological pumping in a 2D system. Here, two independent sets of linearly polarized Raman laser beams that couple two states are applied to create the off-diagonal spin-dependent optical lattices. These lasers have the Rabi frequencies $[\Omega_1 = \Omega_{10}\sin(k_R r_x),\ \Omega_2 = -i\Omega_{20}\cos(k_R r_y)]$, with k_R being the wave vector of the lasers, and $[\Omega'_1 = \Omega'_{10}\cos(k_R r_y),\ \Omega'_2 = i\Omega'_{20}\cos(k_R r_x)]$, respectively, yielding $\Omega_{\mathrm{SO}} = \Omega^*_{10}\Omega_{20}/\Delta_e$ and $V_{Zy0} = \Omega'^*_{10}\Omega'_{20}/\Delta_e$ through Raman processes. In addition, due to the Stark effects, these laser beams generate the spin-independent optical lattices: $-V_x\cos^2(k_R r_x)$ and $-V_y\cos^2(k_R r_y)$ with $V_x = (|\Omega'_{20}|^2 - |\Omega_{10}|^2)/|\Delta_e|$ and $V_y = (|\Omega_{20}|^2 + |\Omega'_{10}|^2)/|\Delta_e|$. In an experiment, one may choose ^{40}K atoms and use a red-detuned laser beam with wavelength 773 nm [43], yielding the recoil energy $E_R = \hbar^2 k_R^2/2m = 2\pi \times 8.3$ kHz. Taking $|\Omega_{20}| = |\Omega'_{20}| = 2\pi \times 0.244$ GHz and $|\Omega_{10}| = |\Omega'_{20}|/3$, we have $V_x = 4.9E_R$, $J_x = 0.08E_R$, and $h_y = -0.72V_{Zy0}$. To implement the pump, we should vary h_y and h_z according to $h_y = 2J_x\cos(\omega t)$ and $h_z = M_0 + 2J_y\sin(\omega t)$ by controlling the strength of the lasers and plugging a π phase appropriately by an acoustic-optical modulator (AOM), and by controlling the frequency of the lasers represented by the green arrows in Fig. 1 as $h_z = \delta/2$, respectively. Note that, when $h_y = 2J_x$, we have $\Omega'_{10} = 0.045\Omega_{20}$ and hence $V_y = 4.9E_R$ (its slight change due to the variation of Ω'_{10} is negligible). For observation, one can measure the *in situ* shift of a cloud of atoms [33,34,45,46] over a cycle, which takes 75 ms if $\omega = 0.01$, much shorter than the lifetime (several seconds) of the achieved topological gases in the experiment [41].

In the 3D case, we can apply two independent sets of the setup proposed in Ref. [30] to realize a Weyl nodal ring. Here, the scheme is optimized by using the linearly polarized laser beams as shown in Figs. 3(c) and 3(d). In the first set, two pairs of Raman processes are utilized to generate the off-diagonal optical lattices. One pair has the Rabi frequencies $[\bar{\Omega}_1 = \bar{\Omega}_{10}\cos(k_{Ly}r_y)e^{-ik_{Lz}r_z/2}$, $\bar{\Omega}_2 = -i\bar{\Omega}_{20}\sin(k_{Lx}r_x)e^{ik_{Lz}r_z/2}]$, and the other pair $[\bar{\Omega}'_1 = \bar{\Omega}_{10}\cos(k_{Ly}r_y)e^{ik_{Lz}r_z/2}$, $\bar{\Omega}'_2 = -i\bar{\Omega}_{20}\sin(k_{Lx}r_x)e^{-ik_{Lz}r_z/2}]$. In the second set, two pairs of Raman laser beams are employed to engineer the other off-diagonal optical lattices. The Rabi frequencies for one pair are $[\tilde{\Omega}_1 = \tilde{\Omega}_{10}\cos(k_{Ly}r_y)e^{-ik_{Lz}r_z/2}$, $\tilde{\Omega}_2 = i\tilde{\Omega}_{10}\cos(k_{Lx}r_x)e^{ik_{Lz}r_z/2}]$, while for the other pair $[\tilde{\Omega}'_1 = \tilde{\Omega}_{10}\cos(k_{Ly}r_y)e^{ik_{Lz}r_z/2}$, $\tilde{\Omega}'_2 = i\tilde{\Omega}_{10}\cos(k_{Lx}r_x)e^{-ik_{Lz}r_z/2}]$. In an experiment, by taking $\tilde{\Omega}_{10} = 2\pi \times 0.14$ GHz and $\bar{\Omega}_{20} = \bar{\Omega}_{10}/4$, we have $V_x \approx V_y \approx 3.2E_R$. Another laser beam is required to create an optical lattice along z with $V_z = 3.2E_R$. Using the geometry of lasers with $k_{Lx} = k_{Ly} = k_{Lz} = \sqrt{4/5}k_R$, we have $J_x = 0.07E_R$ and $h_y = -0.57V_{Zy0}$. Similar to the 2D scenario, the dynamical 4D Weyl nodal ring with the topological pumping can be implemented by tuning h_y and h_z with a period of 86 ms if $\omega = 0.01$.

VI. DISCUSSION AND CONCLUSION

Dynamical Weyl points and dynamical 4D Weyl nodal rings may also be implemented in solid-state materials by applying circularly polarized lights to 2D Dirac materials or 3D nodal-line semimetals, respectively. It allows us to engineer an effective time-independent Hamiltonian obtained by removing the fast-oscillating terms, when the frequency of the light is much larger than other energy scales; this method has been proposed to generate Weyl points from Weyl nodal-line semimetals [47]. Additionally, slowly varying the light intensity allows us to control the Hamiltonian for observation of

the topological pump. Despite the possibility, we have to say that a very exquisite protocol is required to realize dynamical Weyl points and dynamical Weyl nodal rings in solids.

Versatile controllability of cold atoms also manifest in tuning the short-range interactions by Feshbach resonances, which can be tuned to zero. For weak interactions, a mean-field estimate suggests that the interaction may induce a σ_z term [15], thereby shifting the locations of dynamical Weyl points and dynamical 4D Weyl nodal lines and changing the amount of pumped particles. For strong interactions, a previous study suggests that a Weyl point may become Mott gapped while preserving a gapless collective excitation [48]. Whether the value of pumped particles is strongly compromised depends on the density of states around zero energy, which deserves future exploration.

In summary, we have demonstrated the existence of a dynamical Weyl point and dynamical 4D Weyl nodal ring in 2D and 3D systems, respectively. We find that these systems give rise to the nonquantized topological pump and the amount of transported particles can be tuned continuously by controlling experimental parameters, in stark contrast with the Thouless pump with quantized transport. We finally propose an experimental scheme to realize the dynamical Weyl point and dynamical 4D Weyl nodal ring and to observe their corresponding tunable pump, which paves the way for their future experimental observation. Our finding opens a field for studying dynamical gapless phenomena; future direction may include seeking other dynamical gapless phenomena, such as dynamical Yang monopoles.

ACKNOWLEDGMENTS

This work was supported by the start-up program of Tsinghua University (Grant No. 53330300218), National Thousand-Young-Talents Program, and the Ministry of Education and the National Key Research and Development Program of China (Grant No. 2016YFA0301902).

APPENDIX: DERIVATION OF TIGHT-BINDING MODEL

To derive the tight-binding model, let us write down the Hamiltonian in the second quantization language

$$H_{II} = \int d\mathbf{r}\hat{\psi}^{\dagger}(\mathbf{r})H_C\hat{\psi}(\mathbf{r}), \tag{A1}$$

where $\hat{\psi}(\mathbf{r}) = [\hat{\psi}_{\uparrow}(\mathbf{r}),\ \hat{\psi}_{\downarrow}(\mathbf{r})]^T$ with $\hat{\psi}_{\sigma}(\mathbf{r})$ $[\hat{\psi}^{\dagger}_{\sigma}(\mathbf{r})]$ being an annihilation (creation) operator for spin σ $(\sigma = \uparrow, \downarrow)$, which satisfies the anticommutation or commutation relation $[\hat{\psi}_{\sigma}(\mathbf{r}), \hat{\psi}^{\dagger}_{\sigma'}(\mathbf{r}')]_{\pm} = \delta_{\sigma\sigma'}\delta(\mathbf{r}-\mathbf{r}')$ for fermionic atoms $(+)$ or bosonic atoms $(-)$, respectively. The field operator can be approximated by

$$\hat{\psi}_{\sigma}(\mathbf{r}) \approx \sum_{\mathbf{x},\sigma} W_{\mathbf{x}}\hat{c}_{\mathbf{x},\sigma}, \tag{A2}$$

where $W_{\mathbf{x}}$ is the Wannier function for $h_z = V_N = 0$ located at the site $\mathbf{x} = \sum_{\nu} j_{\nu}a_{\nu}\mathbf{e}_{\nu}$ with $\nu = x,\ y$ in 2D ($\nu = x,\ y,\ z$ in 3D) for the lowest band, and $\hat{c}_{\mathbf{x},\sigma}$ is the operator annihilating a particle with spin σ at a site $\mathbf{x}$.

Substituting Eq. (A2) into Eq. (A1) and keeping only the nearest-neighbor hopping terms yields the tight-binding Hamiltonian,

$$\begin{aligned} H_{\mathrm{TB}} = &\sum_{\mathbf{x}}\left[-\sum_{\nu}(J_{\nu}\hat{c}^{\dagger}_{\mathbf{x}}\hat{c}_{\mathbf{x}+a_{\nu}\mathbf{e}_{\nu}} + \mathrm{H.c.}) + h_z\hat{c}^{\dagger}_{\mathbf{x}}\sigma_z\hat{c}_{\mathbf{x}}\right] \\ &+ \sum_{\mathbf{x}} g_{\mathbf{x}}(-J_{\mathrm{SO}}\hat{c}^{\dagger}_{\mathbf{x}}\sigma_y\hat{c}_{\mathbf{x}+a_x\mathbf{e}_x} + \mathrm{H.c.} + h_y\hat{c}^{\dagger}_{\mathbf{x}}\sigma_y\hat{c}_{\mathbf{x}}), \end{aligned} \tag{A3}$$

where $\hat{c}^{\dagger}_{\mathbf{x}} = (\hat{c}^{\dagger}_{\mathbf{x},\uparrow}, \hat{c}^{\dagger}_{\mathbf{x},\downarrow})$ and $g_{\mathbf{x}} = (-1)^{j_x+j_y}$ in 2D [$g_{\mathbf{x}} = (-1)^{j_x+j_y+j_z}$ in 3D]. For more details, we refer to Refs. [15,30] for a derivation of the model and verification of its validity. Using the transformation $\hat{a}_{\mathbf{x}\uparrow} = g_{\mathbf{x}}\hat{c}_{\mathbf{x}\uparrow}$ and $\hat{a}_{\mathbf{x}\downarrow} = \hat{c}_{\mathbf{x}\downarrow}$, we recast the model into the form

$$\begin{aligned} H_{\mathrm{TB}} = \sum_{\mathbf{x}}\Bigg[&\left(\sum_{\nu} J_{\nu}\hat{a}^{\dagger}_{\mathbf{x}}\sigma_z\hat{a}_{\mathbf{x}+a_{\nu}\mathbf{e}_{\nu}} + iJ_{\mathrm{SO}}\hat{a}^{\dagger}_{\mathbf{x}}\sigma_x\hat{a}_{\mathbf{x}+a_x\mathbf{e}_x} + \mathrm{H.c.}\right) \\ &+ h_z\hat{a}^{\dagger}_{\mathbf{x}}\sigma_z\hat{a}_{\mathbf{x}} + h_y\hat{a}^{\dagger}_{\mathbf{x}}\sigma_y\hat{a}_{\mathbf{x}}\Bigg]. \end{aligned} \tag{A4}$$

This Hamiltonian can be written in momentum space as $H_{\mathrm{TB}} = \sum_{\mathbf{k}}\hat{a}^{\dagger}_{\mathbf{k}}H(\mathbf{k})\hat{a}_{\mathbf{k}}$, where $H(\mathbf{k})$ is given in Eq. (7).

[1] X. Wan, A. M. Turner, A. Vishwanath, and S. Y. Savrasov, Phys. Rev. B **83**, 205101 (2011).
[2] K.-Y. Yang, Y.-M. Lu, and Y. Ran, Phys. Rev. B **84**, 075129 (2011).
[3] A. A. Burkov and L. Balents, Phys. Rev. Lett. **107**, 127205 (2011).
[4] G. Xu, H. Weng, Z. Wang, X. Dai, and Z. Fang, Phys. Rev. Lett. **107**, 186806 (2011).
[5] S. A. Yang, H. Pan, and F. Zhang, Phys. Rev. Lett. **113**, 046401 (2014).
[6] A. A. Soluyanov, D. Gresch, Z. Wang, Q. Wu, M. Troyer, X. Dai, and B. A. Bernevig, Nature (London) **527**, 495 (2015).
[7] H. Ishizuka, T. Hayata, M. Ueda, and N. Nagaosa, Phys. Rev. Lett. **117**, 216601 (2016).
[8] C. Fang, L. Lu, J. Liu, and L. Fu, Nat. Phys. **12**, 936 (2016).
[9] M. Gong, S. Tewari, and C. Zhang, Phys. Rev. Lett. **107**, 195303 (2011).
[10] B. M. Anderson, G. Juzeliūnas, V. M. Galitski, and I. B. Spielman, Phys. Rev. Lett. **108**, 235301 (2012).
[11] Y. Xu, R.-L. Chu, and C. Zhang, Phys. Rev. Lett. **112**, 136402 (2014).
[12] T. Dubček, C. J. Kennedy, L. Lu, W. Ketterle, M. Soljačić, and H. Buljan, Phys. Rev. Lett. **114**, 225301 (2015).

[13] B. Liu, X. Li, L. Yin, and W. V. Liu, Phys. Rev. Lett. **114**, 045302 (2015).
[14] Y. Xu, F. Zhang, and C. Zhang, Phys. Rev. Lett. **115**, 265304 (2015).
[15] Y. Xu and L.-M. Duan, Phys. Rev. A **94**, 053619 (2016).
[16] L.-J. Lang, S.-L. Zhang, K. T. Law, and Q. Zhou, Phys. Rev. B **96**, 035145 (2017).
[17] Y. Xu and Y. Hu, arXiv:1807.09732.
[18] L. Lu, L. Fu, J. D. Joannopoulos, and M. Soljačić, Nat. Photonics **7**, 294 (2013).
[19] M. Xiao, W.-J. Chen, W.-Y. He, and C. T. Chan, Nat. Phys. **11**, 920 (2015).
[20] A. A. Burkov, Nat. Mater. **15**, 1145 (2016).
[21] S. Jia, S.-Y. Xu, and M. Z. Hasan, Nat. Mater. **15**, 1140 (2016).
[22] N. P. Armitage, E. J. Mele, and A. Vishwanath, Rev. Mod. Phys. **90**, 015001 (2018).
[23] B. Q. Lv, H. M. Weng, B. B. Fu, X. P. Wang, H. Miao, J. Ma, P. Richard, X. C. Huang, L. X. Zhao, G. F. Chen, Z. Fang, X. Dai, T. Qian, and H. Ding, Phys. Rev. X **5**, 031013 (2015).
[24] S.-Y. Xu, I. Belopolski, N. Alidoust, M. Neupane, G. Bian, C. Zhang, R. Sankar, G. Chang, Z. Yuan, C.-C. Lee, S.-M. Huang, H. Zheng, J. Ma, D. S. Sanchez, B. Wang, A. Bansil, F. Chou, P. P. Shibayev, H. Lin, S. Jia, and M. Z. Hasan, Science **349**, 613 (2015).
[25] L. Lu, Z. Wang, D. Ye, L. Ran, L. Fu, J. D. Joannopoulos, and M. Soljačić, Science **349**, 622 (2015).
[26] K. Deng, G. Wan, P. Deng, K. Zhang, S. Ding, E. Wang, M. Yan, H. Huang, H. Zhang, Z. Xu, J. Denlinger, A. Fedorov, H. Yang, W. Duan, H. Yao, Y. Wu, S. Fan, H. Zhang, X. Chen, and S. Zhou, Nat. Phys. **12**, 1105 (2016).
[27] L. Huang, T. M. McCormick, M. Ochi, Z. Zhao, M.-T. Suzuki, R. Arita, Y. Wu, D. Mou, H. Cao, J. Yan, N. Trivedi, and A. Kaminski, Nat. Mater. **15**, 1155 (2016).
[28] A. A. Burkov, M. D. Hook, and L. Balents, Phys. Rev. B **84**, 235126 (2011).
[29] G. Bian, T.-R. Chang, R. Sankar, S.-Y. Xu, H. Zheng, T. Neupert, C.-K. Chiu, S.-M. Huang, G. Chang, I. Belopolski, D. S. Sanchez, M. Neupane, N. Alidoust, C. Liu, B. Wang, C.-C. Lee, H.-T. Jeng, C. Zhang, Z. Yuan, S. Jia, A. Bansil, F. Chou, H. Lin, and M. Z. Hasan, Nat. Commun. **7**, 10556 (2016).
[30] Y. Xu and C. Zhang, Phys. Rev. A **93**, 063606 (2016).
[31] D.-W. Zhang, Y. X. Zhao, R.-B. Liu, Z.-Y. Xue, S.-L. Zhu, and Z. D. Wang, Phys. Rev. A **93**, 043617 (2016).
[32] D. J. Thouless, Phys. Rev. B **27**, 6083 (1983).
[33] S. Nakajima, T. Tomita, S. Taie, T. Ichinose, H. Ozawa, L. Wang, M. Troyer, and Y. Takahashi, Nat. Phys. **12**, 296 (2016).
[34] M. Lohse, C. Schweizer, O. Zilberberg, M. Aidelsburger, and I. Bloch, Nat. Phys. **12**, 350 (2016).
[35] V. Gritsev and A. Polkovnikov, Proc. Natl. Acad. Sci. USA **109**, 6457 (2012).
[36] X.-L. Qi, T. L. Hughes, and S.-C. Zhang, Phys. Rev. B **78**, 195424 (2008).
[37] D. Xiao, M.-C. Chang, and Q. Niu, Rev. Mod. Phys. **82**, 1959 (2010).
[38] H.-P. Breuer and F. Petruccione, *The Theory of Open Quantum Systems* (Oxford University Press, Oxford, UK, 2007).
[39] L. Zhou, D. Y. Tan, and J. Gong, Phys. Rev. B **92**, 245409 (2015).
[40] Z. Wu, L. Zhang, W. Sun, X.-T. Xu, B.-Z. Wang, S.-C. Ji, Y. Deng, S. Chen, X.-J. Liu, and J.-W. Pan, Science **354**, 83 (2016).
[41] W. Sun, B.-Z. Wang, X.-T. Xu, C.-R. Yi, L. Zhang, Z. Wu, Y. Deng, X.-J. Liu, S. Chen, and J.-W. Pan, arXiv:1710.00717.
[42] X.-J. Liu, K. T. Law, and T. K. Ng, Phys. Rev. Lett. **112**, 086401 (2014).
[43] L. Huang, Z. Meng, P. Wang, P. Peng, S.-L. Zhang, L. Chen, D. Li, Q. Zhou, and J. Zhang, Nat. Phys. **12**, 540 (2016).
[44] Z. Meng, L. Huang, P. Peng, D. Li, L. Chen, Y. Xu, C. Zhang, P. Wang, and J. Zhang, Phys. Rev. Lett. **117**, 235304 (2016).
[45] Y. Qian, M. Gong, and C. Zhang, Phys. Rev. A **84**, 013608 (2011).
[46] L. Wang, M. Troyer, and X. Dai, Phys. Rev. Lett. **111**, 026802 (2013).
[47] Z. Yan and Z. Wang, Phys. Rev. Lett. **117**, 087402 (2016).
[48] T. Morimoto and N. Nagaosa, Sci. Rep. **6**, 19853 (2016).